


Optical injection locking of dual-wavelength midinfrared quantum cascade lasersMohammad M. Sheikhey,¹ Somayeh Kaviani,² and Hamed Baghban^{2,*}¹*Department of Electrical and Computer Engineering, University of Tabriz, Tabriz 5166616471, Iran*²*School of Engineering-Emerging Technologies, University of Tabriz, Tabriz 5166616471, Iran* (Received 22 June 2018; revised manuscript received 11 September 2018; published 7 November 2018)

Multiwavelength quantum cascade lasers (QCLs) as coherent optical sources at mid- and far-IR spectral regions can be tailored regarding their dynamic and modulation response, output power, and stability condition of each spectral component under optical injection locking. Based on a developed model fitted to experimental data of a dual-wavelength mid-infrared (mid-IR), we show that an injection ratio threshold exists for each wavelength after which a stable-locking is obtained. While the uninjected wavelength imposes a long turn-on delay and an increased threshold current before its extinction, the injection-locked wavelength may experience output powers and modulation bandwidths about twice as large as the free-running values at moderate injection ratios. This idea provides a tunability viewpoint for spectral and power-dependent switching applications of multiwavelength and broadband QCLs.

DOI: [10.1103/PhysRevA.98.053810](https://doi.org/10.1103/PhysRevA.98.053810)**I. INTRODUCTION**

Quantum cascade lasers in their third decade of appearance are maintaining the evolutionary route toward multiwavelength, high-power, and room-temperature performances beside their celebrated applications as mid-infrared (mid-IR) and terahertz sources.

Development of multiwavelength and broadband quantum cascade lasers (QCLs) are especially promising for spectroscopic applications such as trace gas spectroscopy, environmental monitoring, medical sensing systems, and security process monitoring applications [1–3]. Broadband QCLs can considerably enhance the Fourier-transform infrared spectrometers by replacing their traditional thermal sources, which provide relatively low infrared power and limit the characterization of low-absorptivity materials [4]. On the other hand, raised from the giant nonlinearities of quantum well structures, multiwavelength QCLs have found importance for nonlinear light generation through difference frequency generation [5], second harmonic, and sum-frequency generation [6].

Multiwavelength and broadband emission from QCLs are typically achieved through different approaches, including external cavity (EC) configuration [7,8], midinfrared frequency comb generation [9], integration of different cascade sections with each section lasing at a slightly different wavelength [10], heterogeneous cascading of multiple substacks emitting at different wavelengths [11,12], and homogeneous design of the active region by engineering the number of optical transitions [13–15]. Together with the advances in the development of multiwavelength quantum cascade sources, investigations have been carried out to pave the way for achieving mode spacing tunability, selective output power control, and operation under the same driving conditions of

dual and multiwavelength QCLs. The latter condition, as an instant, requires flawless design of the active region while considering the serious effects of the waveguide loss and the temperature compensation at longer wavelengths. The investigations were initiated by the “tap”-into-the-cascade design for a QCL based on heterogeneous cascading of two substacks for two-wavelength operations (5.2 μm and 8 μm) [11]. This exploited feature provides the selective manipulation of the laser threshold of one substack while keeping the other wavelength undisturbed. Also, a stable and robust pulsed regime over the full dynamic range of the injection currents has been attained through active mode locking of an EC QCL [16].

Optical injection locking (OIL) of QCLs, as an experimental technique for synchronizing two coupled lasers, enables stabilization and tuning of the round-trip frequency [9,17], improvement of the noise behavior, and modulation bandwidth of a laser [18,19]. The effect of OIL on the stability of a master-slave laser system can be interpreted in terms of a generalized mathematical model for synchronization of a two-generator system [20].

Despite the numerous investigations performed on injection-locked QCLs, injection-locked multiwavelength QCLs have received less attention compared with their solid-state and fiber multiwavelength counterparts.

A dual-wavelength injection-locked system consisting of two independent master lasers locked on specific longitudinal modes of a Ti:sapphire laser has been reported to yield full controllability of the relative pulsed energies while the pulsed outputs fully overlap in time. Flexible selectivity and wide frequency scanning of the two wavelengths have also been achieved [21]. For fiber lasers with multilongitudinal modes (MLM), injection locking can yield widely tunable single-frequency lasing characteristics by decreasing the number of longitudinal modes and narrowing the linewidth of the injected MLM laser output [22]. Therefore, a switchable single frequency operation with considerable side-mode suppression ratio can be obtained over the whole wavelength

*h-baghban@tabrizu.ac.ir

tuning range. Multiwavelength injection locking in semiconductor lasers has also been utilized in optical communications for wavelength division multiplexing (WDM) networks. A Fabry-Perot laser diode (FP-LD) as a multiwavelength laser and injection-locked with 8 WDM wavelengths has been demonstrated as an 8×10 Gb/s multiple wavelength converter [23]. Such an idea can reduce the number of wavelength converters and enables simultaneous broadcasting of multiple wavelengths. Multiwavelength monitoring in a WDM system based on injection-locked FP-LD has also been reported as an efficient and cost-effective method where injection to one of the longitudinal modes of the FP-LD suppresses the whole Fabry-Perot mode comb [24]. The idea of suppressing a dominant mode using OIL has been utilized for all-optical signal processing based on all-optical gates where multi-input (multiwavelength) injection locking efficiently suppresses the dominant mode of a FP-LD [25]. Also, using multiwavelength injection locking of FP-LDs has been proposed to achieve a colorless WDM-passive optical network (WDM-PON) transmission where multiwavelength light sources in C and L bands lock the FP lasers at a subscriber site and a central office [26].

Here, we have developed a theoretical model to examine an injection-locked homogeneous dual-wavelength mid-infrared quantum cascade laser. The output wavelengths at $\lambda_1 = 10.5 \mu\text{m}$ and $\lambda_2 = 8.9 \mu\text{m}$ have a close threshold condition ($I_{\text{th1}}/I_{\text{th2}} = 1.07$), so the gain competition before and after the injection locking determine the behavior of each wavelength. Single-wavelength emission criteria and the modulation bandwidth characterization for applications such as free-space communication are discussed. Free-running power-current characteristics of the dual-wavelength QCL have been fitted to an experimental dual-wavelength laser through a developed rate-equation-based model to ensure the experimental reliability of the model. The P-I characteristics of the developed model agree well with the experimental P-I behavior of the dual-wavelength midinfrared QCL reported in Ref. [27]; therefore, a good measure of the effect of OIL on lasing characteristics can be obtained through the rate equation model. Finally, the stability condition, dynamic, and modulation response of each wavelength have been studied based on the so-called injection ratio threshold.

II. MODEL DESCRIPTION

Our conducted investigation is based on a four-level gain medium illustrated schematically in Fig. 1, where the two laser lines share a common upper level and the model can describe the mode interactions due to mutual gain depletion. To simplify the carriers and photons dynamics, two electromagnetically decoupled photon modes have been assumed here by neglecting optical nonlinearities and the rate equations describing the system dynamics are given as follows [18,27–29]:

$$\begin{aligned} \dot{N}_4 &= WLJ/e - N_4/\tau_4 - g^{(1)}(N_4 - N_3)S^{(1)} \\ &\quad - g^{(2)}(N_4 - N_2)S^{(2)}, \end{aligned} \quad (1)$$

$$\dot{N}_3 = N_4/\tau_{43} - N_3/\tau_3 + g^{(1)}(N_4 - N_3)S^{(1)}, \quad (2)$$

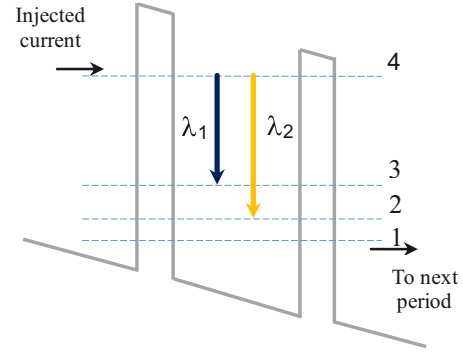


FIG. 1. The energy-level diagram of one stage of the active region. Lasing takes place simultaneously through transitions from level 4 to level 3, corresponding to $\lambda_1 = 10.5 \mu\text{m}$ and from level 4 to level 2, corresponding to $\lambda_2 = 8.9 \mu\text{m}$ wavelengths. The lower lasing level is depleted to level 1 through the LO-phonon emission.

$$\dot{N}_2 = N_4/\tau_{42} + N_3/\tau_{32} - N_2/\tau_{21} + g^{(2)}(N_4 - N_2)S^{(2)}, \quad (3)$$

$$\dot{N}_1 = N_4/\tau_{41} + N_3/\tau_{31} + N_2/\tau_{21} - N_1/\tau_{\text{out}}, \quad (4)$$

$$\begin{aligned} \dot{E}^{(1)} &= 1/2(N_p g^{(1)}(N_4 - N_3) - 1/\tau_p^{(1)})(1 + j\alpha_H^{(1)})E(t)^{(1)} \\ &\quad + k_c A_{\text{inj}}^{(1)} - j\omega_{\text{inj}}^{(1)}E(t)^{(1)}, \end{aligned} \quad (5)$$

$$\begin{aligned} \dot{E}^{(2)} &= 1/2(N_p g^{(2)}(N_4 - N_2) - 1/\tau_p^{(2)})(1 + j\alpha_H^{(2)})E(t)^{(2)} \\ &\quad + k_c A_{\text{inj}}^{(2)} - j\omega_{\text{inj}}^{(2)}E(t)^{(2)}. \end{aligned} \quad (6)$$

In the above equations, J denotes the electron current density pumped into the upper level, e is the electron charge, W and L are the lateral dimensions of the cavity, N_p is the number of gain stages, L_p is the thickness of a stage, $V = N_p W L L_p$ is the volume of the active area, N_j is the carrier numbers of the j th state, $E^{(i)}(t) = S^{(i)}(t)^{1/2} \exp(j\varphi^{(i)})$ is the complex electric field of the i th mode where the phase difference between the slave and master lasers is given by $\varphi^{(i)} = \varphi_{\text{slave}}^{(i)} - \varphi_{\text{master}}^{(i)}$, and $A_{\text{inj}} = S_{\text{inj}}^{1/2}$ is the injected field magnitude where $S_{\text{inj}} = R_{\text{inj}} \times S_{\text{fr}}$ is the number of injected photons with injection ratio of R_{inj} and free-running photon number of S_{fr} . Also, $\omega_{\text{inj}}^{(i)}$ is the frequency detuning defined as $\omega_{\text{inj}}^{(i)} = \omega_{\text{master}}^{(i)} - \omega_{\text{slave}}^{(i)}$, α_H is the linewidth enhancement factor (LEF), $g^{(i)} = \Gamma^{(i)} c' \sigma^{(i)} / V$ is the gain coefficient of the i th mode where $c' = c/n_{\text{eff}}$ is the speed of light, n_{eff} is the cavity effective index, and stimulated emission cross sections are defined as $\sigma^{(i)} = 4\pi(ez^{(i)})^2 / \epsilon_0 n_{\text{eff}} \lambda_i (2\gamma^{(i)})$, where z is the dipole matrix element of the transition and 2γ stands for the full width at half maximum of the i th transition, k_c is the coupling rate of the master laser into the slave laser defined by $k_c = c(1 - R)/(2n_{\text{eff}} L R^{1/2})$, where R is the facet reflectivity of the slave laser at injected-side and L is the slave laser cavity length. The carrier scattering times between the states are determined with τ_{mn} . For simplicity, we have defined $1/\tau_4 = 1/\tau_{43} + 1/\tau_{42} + 1/\tau_{41}$ and $1/\tau_3 = 1/\tau_{32} + 1/\tau_{31}$. Finally, the radiative spontaneous emission time constant can be described as $\tau_{\text{sp}}^{(i)} = \epsilon_0 \hbar \lambda_i^3 / 8\pi^2 n_{\text{eff}} (ez^{(i)})^2$, $\tau_p^{(i)}$ is the photon lifetime,

and $\beta^{(i)}$ is the spontaneous emission factor of the i th mode [27,28]. Considering $I = WLJ/e$, introducing small signal variation of I as $I + \Delta I$ results in the small carrier and complex electric field (also photon number and the phase difference between the slave and master lasers) fluctuations around the steady-state values as follows [18]:

$N_i(t) = N_i + \Delta N_i(t)$, $E(t)^{(i)} = E^{(i)} + \Delta E(t)^{(i)}$, $S(t)^{(i)} = S^{(i)} + \Delta S(t)^{(i)}$, and $\varphi(t)^{(i)} = \varphi^{(i)} + \Delta\varphi(t)^{(i)}$. Inserting these definitions into Eqs. (1)-(6) and considering $\Delta E(t)^{(i)} = E^{(i)}(\Delta S(t)^{(i)}/2S^{(i)} + j\Delta\varphi(t)^{(i)})$ [18], an 8×8 small signal variation matrix can be obtained as below:

$$(a)_{8 \times 8}(\Delta)_{8 \times 1} = (\Delta I)_{8 \times 1},$$

$$\Delta_{8 \times 1}(\omega) = [\Delta N_4 \ \Delta N_3 \ \Delta N_2 \ \Delta N_1 \ \Delta S_2 \ \Delta S_1 \ \Delta\varphi_2 \ \Delta\varphi_1]^T,$$

$$\Delta I_{8 \times 1}(\omega) = [1 \ 0 \ 0 \ 0 \ 0 \ 0 \ 0 \ 0]^T, \quad (7)$$

where $a_{ii} = \gamma_{ii} + j\omega$; $\gamma_{11} = g^{(1)}S^{(1)} + g^{(2)}S^{(2)} + 1/\tau_4$; $a_{13} = -g^{(2)}S^{(2)}$; $a_{15} = -g^{(2)}(N_4 - N_2)$; $a_{16} = -g^{(1)}(N_4 - N_3)$; $a_{21} = -g^{(1)}S^{(1)} - 1/\tau_{43}$; $\gamma_{22} = g^{(1)}S^{(1)} + 1/\tau_3$; $a_{26} = -g^{(1)}(N_4 - N_3)$; $a_{31} = -g^{(2)}S^{(2)} - 1/\tau_{42}$; $a_{32} = -1/\tau_{32}$; $\gamma_{33} = g^{(2)}S^{(2)} + 1/\tau_{21}$; $a_{35} = -g^{(2)}(N_4 - N_2)$; $a_{41} = -1/\tau_{41}$; $a_{42} = -1/\tau_{31}$; $a_{43} = -1/\tau_{21}$; $\gamma_{44} = 1/\tau_{21}$; $a_{51} = -N_p g^{(2)}S^{(2)} - N_p \beta^{(2)}/\tau_{sp}^{(2)}$; $a_{53} = N_p g^{(2)}S^{(2)}$; $\gamma_{55} = 0.5(1/\tau_{ph}^{(2)} - N_p g^{(2)}(N_4 - N_2))$; $a_{57} = -2S^{(2)}\omega_{inj}^{(2)} + \alpha_H^{(2)}S^{(2)}$; $(N_p g^{(2)}(N_4 - N_2) - 1/\tau_{ph}^{(2)})$; $a_{61} = -N_p g^{(1)}S^{(1)} - N_p \beta^{(1)}/\tau_{sp}^{(1)}$; $a_{62} = N_p g^{(1)}S^{(1)}$; $\gamma_{66} = 0.5(1/\tau_{ph}^{(1)} - N_p g^{(1)}(N_4 - N_3))$; $a_{68} = -2S^{(1)}\omega_{inj}^{(1)} + \alpha_H^{(1)}S^{(1)}$; $(N_p g^{(1)}(N_4 - N_3) - 1/\tau_{ph}^{(1)})$; $a_{71} = -\alpha_H^{(2)}N_p g^{(2)}/2$; $a_{73} = \alpha_H^{(2)}g^{(2)}/2$; $a_{75} = -(\alpha_H^{(2)}/4S^{(2)})N_p g^{(2)}$; $(N_4 - N_2) + (\omega_{inj}^{(2)}/2S^{(2)})$; $\gamma_{77} = 0.5(1/\tau_{ph}^{(2)} - N_p g^{(2)}(N_4 - N_2))$; $\gamma_{81} = \alpha_H^{(1)}N_p g^{(1)}/2$; $\gamma_{82} = -\alpha_H^{(1)}g^{(1)}/2$; $\gamma_{86} = (\alpha_H^{(1)}/4S^{(1)})N_p g^{(1)}$; $(N_4 - N_3) - (\omega_{inj}^{(1)}/2S^{(1)})$; $\gamma_{88} = 0.5(1/\tau_{ph}^{(1)} - N_p g^{(1)}(N_4 - N_3))$.

The normalized transfer function of the modulation response can be obtained by

$$H(\omega)^{(i)} = \frac{S^{(i)}(\omega)/\Delta I(\omega)}{H(0)^{(i)}} = \frac{\prod_m k_m(j\omega - z_m)}{\prod_n l_n(j\omega - p_n)}. \quad (8)$$

z_m and p_n correspond to the roots of the nominator polynomial (zeros) and denominator polynomial (poles), respectively. The following structural and physical parameters have been used in the developed model [27,28]: $\tau_{43} = 12.5$ ps, $\tau_{42} = 2.3$ ps, $\tau_{41} = 2.1$ ps, $\tau_{32} = 3$ ps, $\tau_{31} = 0.15$ ps, $\tau_{21} = 0.18$ ps, $\tau_{sp}^{(1)} = 66$ ns, $\tau_{sp}^{(2)} = 30$ ns, $\tau_{out} = 0.98$ ps, $\tau_p^{(1)} = 9.5$ ps, $\tau_p^{(2)} = 9.3$ ps, $\beta^{(1)} = \beta^{(2)} = 2 \times 10^{-3}$, $R = R_1 = R_2 = 0.29$, $L = 1$ mm, $W = 24$ μ m, $L_p = 60$ nm, $N_p = 30$, $g^{(1)} = 1550$ s $^{-1}$, $g^{(2)} = 1792$ s $^{-1}$. Due to small values of LEF in QCLs, $\alpha_H^{(1)} = \alpha_H^{(2)} = 0$ have been considered for simplicity.

It should be noted that all the time and frequency domain data discussed in Sec. III (either in the free-running or in the injection-locked QCL) have been obtained from the steady-state results of the dynamic response of the rate equations.

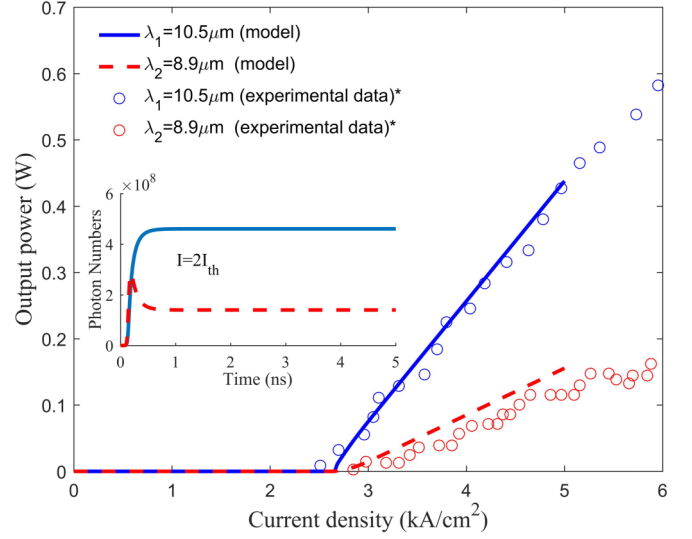


FIG. 2. P-I characteristics of the dual-wavelength QCL. The solid curves correspond to the obtained data from the developed model. *The circle-marked curves present the data extracted from Ref. [27]. Inset illustrates the dynamic responses of photon numbers for the first and the second wavelengths at $I = 2I_{th}$.

III. RESULTS AND DISCUSSION

The P-I characteristics of the developed model have been presented in Fig. 2, where a good agreement is obtained with the experimental characteristics of the dual-wavelength midinfrared QCL reported in Ref. [27]. A threshold current ratio of ~ 1.07 has been achieved between the emission wavelengths. Bias currents up to $2 \times I_{th}$ (threshold current of λ_1) have been assumed in this study where the experimental data supports the developed theoretical model. So, a comprehensive view of the effect of injection locking on lasing characteristics can be obtained through the developed rate equation model. Therefore, the modulation response, stable-locked/stable-unlocked/unstable operation criteria, and the injection-dependant properties of the QCL can be determined by the locations of zeros and poles of the transfer function of the modulation response. Stability analysis based on the poles of the function is performed at first to obtain the stability boundaries and locking map of the laser in this section.

Then, based on the calculated zero-pole locations, we justify the modulation response and the injection threshold of the slave laser. Dynamics of photon populations for both wavelengths are also presented to further clarify the injection-related characteristics of each wavelength.

To investigate the injection-locking behavior of the dual-wavelength QCL, the locking map of the laser, including the stable-locked, stable-unlocked, and unstable regions have been determined for λ_1 . Since the locking process of λ_2 would lead to similar outcomes, the results have not been discussed to avoid redundancy. The first criterion for stability, which comes from the carrier-induced frequency shift, determines the stable-locking boundaries for a QCL just similar to a laser diode. The phase values for the negative and positive detuning edges correspond to $\cot g^{-1}\alpha$ and $-\pi/2 - t g^{-1}\alpha$,

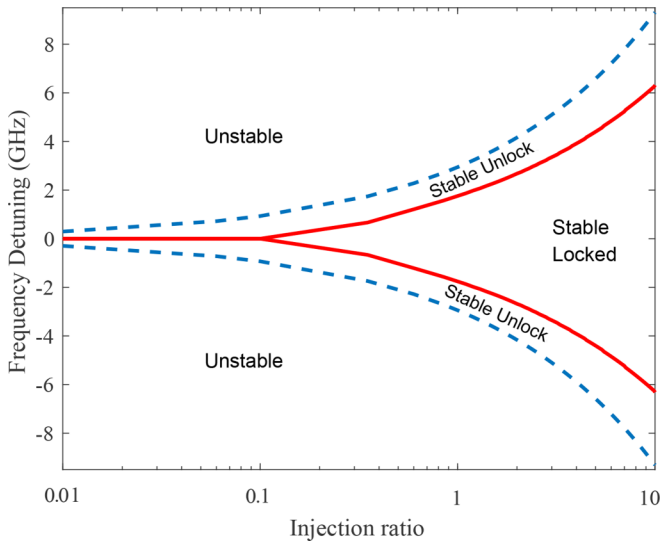


FIG. 3. Optical injection-locking diagram as a function of the frequency detuning for λ_1 at $I = 2 I_{th}$. Solid and dashed curves represent the boundaries of stable-locked/stable-unlocked and stable-unlocked/unstable regions, respectively.

respectively, where the QCL is in stable lasing condition [29,30]. However, the second criterion corresponds to the region in which the output power for λ_2 can be neglected. This region denotes the stable-locking region of λ_1 , where the slave laser follows the master and a single frequency output is achieved.

As is clear in Fig. 3, the stable-locking region is considerably limited compared to the conventional QCLs where the laser is stably locked at low injection ratios [29].

Since OIL directly manipulates the photon populations of both wavelengths which are connected through the carrier population in level 4, the output powers and the threshold currents of each wavelength are consequently affected by the injection strength. To give a measure, the P-I characteristics of the free-running laser have been compared to the injected results at different injection ratios in Fig. 4(a). The meaningful reduction of the threshold current of injection-locked wavelength (λ_1) at the hands of the increase of the threshold current for the second wavelength (λ_2) clearly denotes the carrier dynamics in the active region. The normalized threshold current for the injection-locked wavelength further decreases by the injection ratio and can reach to $<0.5 \times I_{th1}$ at large injection ratios as illustrated in Fig. 4(b) while the normalized threshold current for λ_2 can increase up to $\sim 2.5 \times I_{th2}$.

To determine the stable-locking boundaries at which the λ_2 photons become negligible, an injection-ratio-dependant output power and 3dB modulation bandwidth have been demonstrated in Fig. 5. Increasing the injection ratio, as illustrated in Fig. 5, reduces the λ_2 photons while λ_1 becomes the dominant emitting wavelength for injection ratios larger than a threshold of ~ 0.15 . This injection ratio threshold (R_{th}) is also a function of the frequency detuning, as can be inferred from Fig. 3. Due to lower photon numbers of λ_2 , a larger injection ratio threshold and narrower stable-locked region are expected as well. Stemmed from the output behavior of the λ_1 before and after

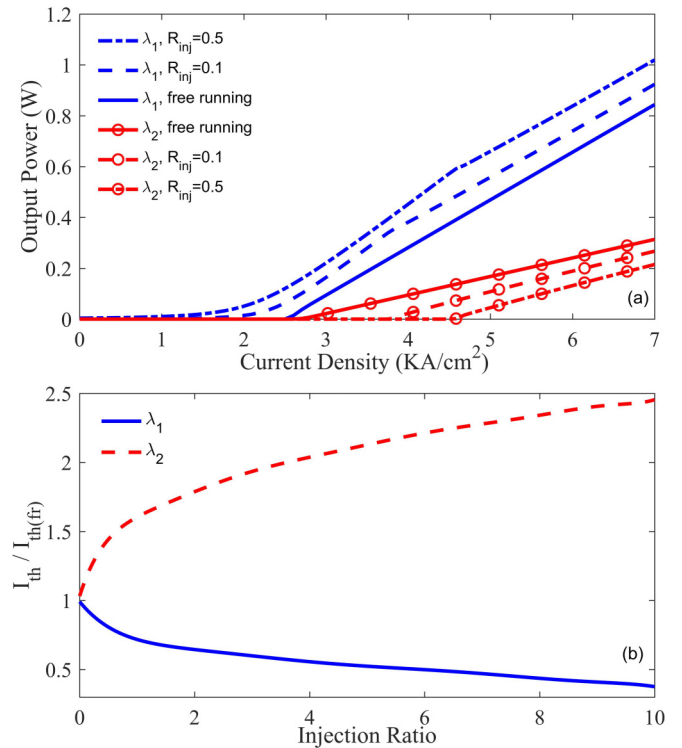


FIG. 4. (a) The output power and current density curves for both wavelengths at different injection ratios of the first wavelength (λ_1), (b) The normalized threshold current of the λ_1 and λ_2 wavelengths at different injection ratios and $S_{inj} = R_{inj} \times S_{fr1}$ where S_{fr1} is free-running photon numbers λ_1 at $I = 1.2 \times I_{th1}$ of (frequency detuning of zero has been considered).

the injection threshold, the 3dB-bandwidth characteristics of the laser show different trends around the injection threshold. As expected from the injected-locked QCL, an increase in the injection ratio enhances the 3dB modulation bandwidth in the stable-locked region of QCL. However, as illustrated in Fig. 5, the 3dB bandwidth enhancement in the stable-unlocked region (before R_{th}) is considerably higher than the stable-locked region. To address this characteristic, injection-ratio-dependent zeros and poles (the first and the second zeros and poles of the transfer function of the modulation response) have been depicted in Fig. 6. Increasing the injection ratio up to R_{th} shifts the first zero and poles toward lower frequencies. The first zero and pole are in their closest position to the $j\omega$ axis at $R_{inj1} = R_{th1} \cong 0.15$, which means that their effect is more pronounced. This effect is obvious from the modulation response illustrated in Fig. 7(b), where a rapid rise in the frequency behavior clearly shows the shift of zeros of the transfer functions. It should be noted that the other zeros and poles also shift toward lower frequencies as depicted for the second zero and pole in Fig. 6 (lower panel). The zero frequency can reach to even a few MHz (<10 MHz around R_{th}) and results in an intense overshoot in the modulation response of the system. For injection ratios larger than R_{th} , the first and the second zeros and poles coincide and cancel each other out. Thus, the modulation bandwidth is determined by the poles of the transfer function at higher frequencies (third and fourth poles). This effect can be verified by the modulation

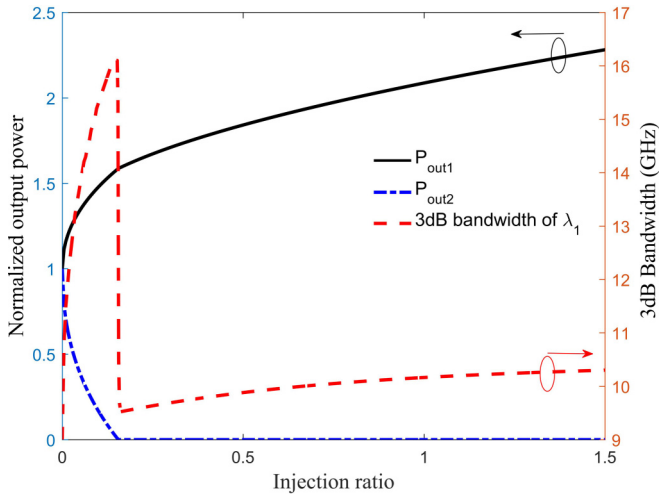


FIG. 5. Left axis: Output powers of the λ_1 and λ_2 wavelengths at $I = 2 I_{th}$ normalized to the free-running output power of each wavelength at different injection ratios. Right axis: 3dB modulation bandwidth of the λ_1 wavelength at $I = 2 I_{th}$ and different injection ratios.

responses presented in Figs. 7(b) and 7(c). To further elaborate the modulation response of the injection-locked slave laser, the modulation characteristics of the free-running laser along with the injection-locked λ_1 and λ_2 responses have been depicted in Fig. 7(a). Results obtained for $1.5 I_{th}$ and $2 I_{th}$ in the free-running condition demonstrate that the 3dB modulation bandwidth for λ_1 is larger than λ_2 due to larger slope efficiency and the output power of the λ_1 as illustrated in Fig. 2. However, the 3dB modulation bandwidths approach each other by increasing the bias current while a considerable

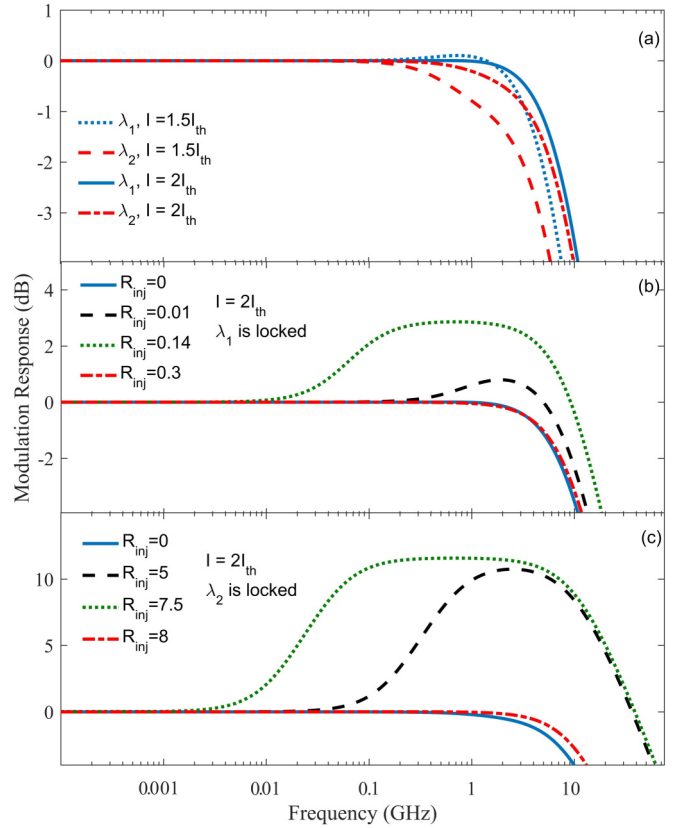


FIG. 7. Modulation response of the (a) free-running dual-wavelength QCL at $I = 1.5 I_{th}$ and $I = 2 I_{th}$, (b) optical injection-locked λ_1 wavelength at $I = 2 I_{th}$, zero detuning, and different injection ratios, (c) optical injection-locked λ_2 wavelength at $I = 2 I_{th}$, zero detuning and different injection ratios.

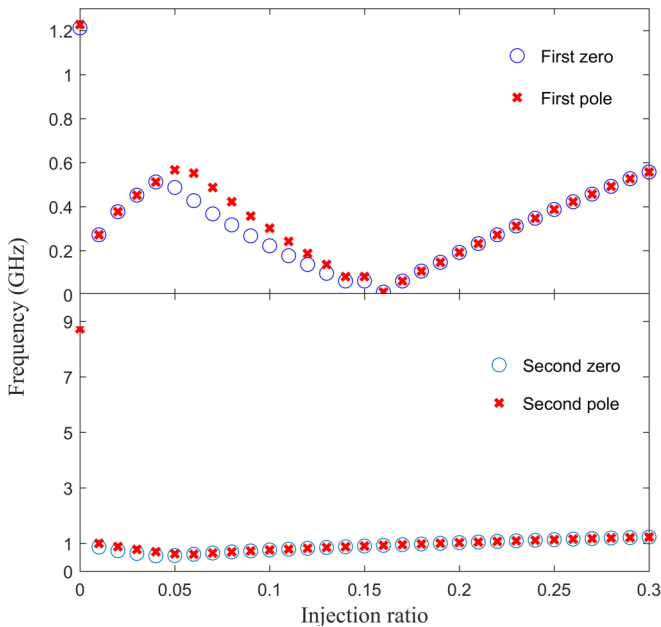


FIG. 6. Frequency location versus injection ratio of the first and the second zeros and poles extracted from the transfer function of the modulation response of the λ_1 wavelength at $I = 2 I_{th1}$ and zero-frequency detuning.

distinction can be seen at lower bias currents. The modulation response of the injection-locked λ_2 is displayed in Fig. 7(c) for free-running, stable-unlocked, and stable-locked conditions. The larger injection ratio threshold for λ_2 ($R_{th2} \sim 0.15$ and $R_{th2} \sim 7.5$) is due to the larger photon numbers of λ_1 , compared to λ_2 in free-running mode. Additionally, it can be inferred that lower injection-ratio thresholds are required for lower bias currents.

In addition to the decrease in the output power of λ_2 for injection-locked λ_1 mode, the turn-on delay (ToD, defined as the time that elapses between the moment the bias is applied and the time that the photon number reaches 10% of its steady-state value) of λ_2 is also affected significantly. As depicted in Fig. 8, ToDs from ~ 0.05 ns to ~ 12 ns are obtained, corresponding to injection ratios of 0.01 to 0.15 (R_{th1}). The inset of Fig. 8 illustrates the dynamic response of the normalized output power for λ_2 (normalized to the free-running output power of λ_2). The output power of λ_2 is almost negligible to measure the ToD beyond the R_{th1} .

Besides the wavelength selectivity, the power, and modulation bandwidth characteristics of the injection-locked wavelength, simultaneous injection locking of both wavelengths may modify the output characteristics of each wavelength in a different manner regarding the photon populations. To further discuss this case, the free-running and locked states

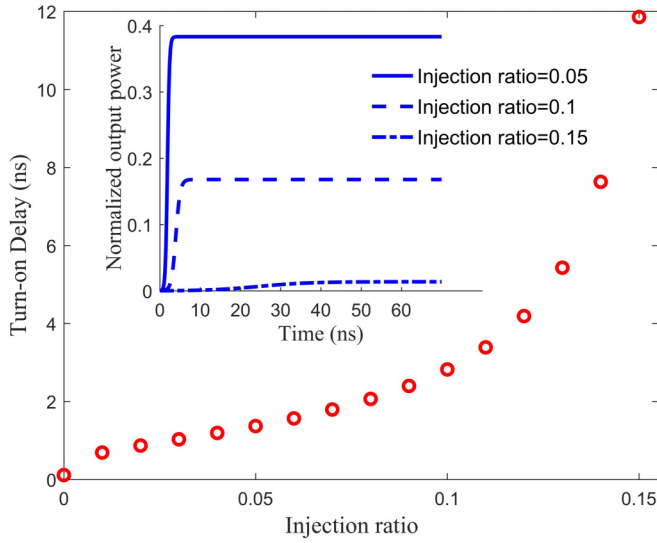


FIG. 8. Turn-on delay of the λ_2 wavelength at $I = 2 I_{th2}$ and different injection ratios (λ_1 is injection locked). Inset illustrates the corresponding dynamics of the normalized output power of λ_2 at three sample injection ratios of 0.05, 0.1, and 0.15.

of each wavelength compared to the simultaneous locked state have been depicted in Fig. 9. Since injection locking reduces the carrier number in level 4 and also the modal gain, negligible photon numbers at λ_2 are obtained for injection-locked λ_1 case, which is further reduced for larger injection ratios of λ_{-1} [$S_2 \sim 600$ at $R_{inj1} = 1$ illustrated by solid curves in Figs. 9(a) and 9(b)]. The modulation bandwidth of the λ_1 experiences an increase with respect to the free-running condition at the same time [solid curve in Fig. 9(c)]. Similarly, an injection-locked λ_2 leads to larger photon numbers at this wavelength while a severe reduction at λ_1 photon numbers and modulation bandwidth are observed (dotted curves in Fig. 9). Since the number of λ_1 photons are still large enough and the system operates in the stable-unlocked condition, an overshoot followed by a considerable increase of the 3dB modulation bandwidth is observed in the modulation response of λ_2 .

When both wavelengths are injected, different conditions for photon numbers and stability situations of the system are observed based on values of S_1 and S_2 . For $R_{inj1} = R_{inj2} = 1$ ($S_1 > S_2$), the photon numbers lie between the free-running and the injection-locked values for each wavelength and the stability criteria is determined by λ_1 (frequency detuning of λ_2 doesn't limit the stability conditions). A similar behavior is obtained for $S_2 > S_1$ for the injection-locked operation of both wavelengths. Also, for $S_1 \sim S_2$, the stability criteria is determined by both wavelengths.

The output power of the laser as a function of the bias current in the free-running and two different injection ratios of $R_{inj1} = R_{inj2} = 0.5$ and $R_{inj1} = R_{inj2} = 1$ have been illustrated in Fig. 9(e), which reveals the effect of injection locking of both wavelengths on the threshold current. Threshold current densities of λ_1 and λ_2 clearly decrease with increasing the corresponding injection ratio.

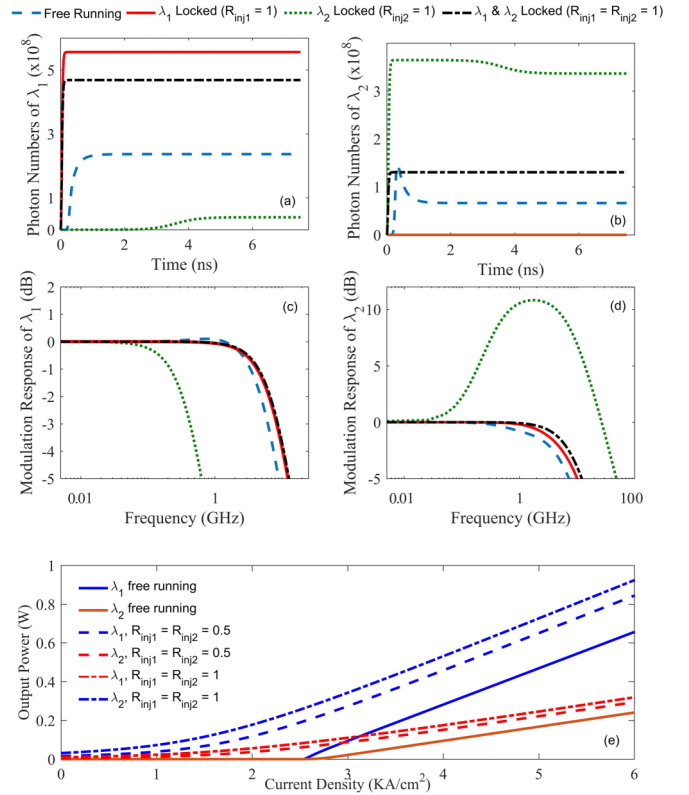


FIG. 9. Photon numbers, modulation response, and power-current characteristics of the injection-locked dual-wavelength QCL at $1.5 I_{th}$.

IV. CONCLUSIONS

The OIL concept of multiwavelength QCLs was studied using the developed model of a homogeneous dual-wavelength midinfrared QCL emitting at $10.5 \mu\text{m}$ and $8.9 \mu\text{m}$ wavelengths. It was shown that the stable-locking region of the dual-wavelength QCL is limited significantly compared to conventional QCLs. An injection ratio threshold was defined, after which the uninjected wavelength is negligible and the modulation bandwidth of the injection-locked wavelength demonstrates a different trend compared to lower injection ratios. Based on an injection-ratio-dependent zero-pole analysis, the modulation response was investigated in the stable-locked and -unlocked regions. Injection ratios close to injection-ratio threshold resulted in large overshoot in the modulation response while a flat modulation response was obtained for larger injection ratios. The normalized threshold current of the injection-locked wavelength, on the other hand, exhibited a decreasing tendency with the injection ratio and reached to below $0.5 \times I_{th1}$ at large injection ratios while the normalized threshold current for the uninjected wavelength increased up to $\sim 2.5 \times I_{th2}$. The uninjected wavelength also imposed a large turn-on delay of ~ 12 ns and a severe power reduction before its extinction at the injection-ratio threshold. This tunability method can be generalized for multiwavelength QCLs regarding their spectral and power-dependent characteristics.

- [1] A. Hugi, R. Terazzi, Y. Bonetti, A. Wittmann, M. Fischer, M. Beck, J. Faist, and E. Gini, *Appl. Phys. Lett.* **95**, 061103 (2009).
- [2] J. Jagerska, P. Jouy, A. Hugi, B. Tuzson, H. Looser, M. Mangold, M. Beck, L. Emmenegger, and J. Faist, *Appl. Phys. Lett.* **105**, 161109 (2014).
- [3] R. F. Curl, F. Capasso, C. Gmachl, A. A. Kosterev, B. McManuse, R. Lewicki, M. Pusharsky, G. Wysockic, and F. K. Tittel, *Chem. Phys. Lett.* **487**, 1 (2010).
- [4] L. Diehl, C. Pflugl, M. Witinski, P. Wang, T. Tague, and F. Capasso, CLEO: Applications, San Jose, California, JThB1 (2010), doi:10.1364/CLEO.2010.JThB1.
- [5] T. Onose and M. Katsuragawa, *Opt. Express* **15**, 1600 (2007).
- [6] N. Owschimikow, C. Gmachl, A. Belyanin, V. Kocharovskiy, D. L. Sivco, R. Colombelli, F. Capasso, and A. Y. Cho, *Phys. Rev. Lett.* **90**, 043902 (2003).
- [7] A. Hugi, R. Maulini, and J. Faist, *Semicond. Sci. Technol.* **25**, 083001 (2010).
- [8] G. Luo, C. Peng, H. Q. Le, S.-S. Pei, H. Lee, W.-Y. Hwang, B. Ishaug, and J. Zheng, *IEEE J. Quantum Electron.* **38**, 486 (2002).
- [9] A. Hugi, G. Villares, S. Blaser, H. C. Liu, and J. Faist, *Nature* **492**, 229 (2012).
- [10] C. Gmachl, D. L. Sivco, R. Colombelli, F. Capasso, and A. Y. Cho, *Nature* **415**, 883 (2002).
- [11] C. Gmachl, D. L. Sivco, J. N. Baillargeon, A. L. Hutchinson, F. Capasso, and A. Y. Cho, *Appl. Phys. Lett.* **79**, 572 (2001).
- [12] S. P. Khanna, M. Salih, P. Dean, A. G. Davies, and E. H. Linfield, *Appl. Phys. Lett.* **95**, 181101 (2009).
- [13] M. I. Hossain, Y. Wang, A. Belyanin, D. L. Sivco, A. M. Sergent, and O. Malis, *Proc. SPIE* **8277**, 82770R (2012).
- [14] K. Fujita, T. Edamura, S. Furuta, and M. Yamanishi, *Appl. Phys. Lett.* **96**, 241107 (2010).
- [15] B. Mirzaei, A. Rostami, and H. Baghban, *Opt. Laser Technol.* **44**, 378 (2012).
- [16] D. G. Revin, M. Hemingway, Y. Wang, J. W. Cockburn, and A. Belyanin, *Nat. Commun.* **7**, 11440 (2016).
- [17] M. R. St-Jean, M. I. Amanti, A. Bernard, A. Calvar, A. Bismuto, E. Gini, M. Beck, J. Faist, H. C. Liu, and C. Sirtori, *Laser Photon. Rev.* **8**, 443 (2014).
- [18] M. M. Sheikhey, M. Goudarzi, R. Yadipour, and H. Baghban, *J. Opt. Soc. Am. B* **33**, D57 (2016).
- [19] C. Juretka, H. Simos, A. Bogris, D. Syvridis, W. Elsaber, and M. Carras, *IEEE J. Quantum Electron.* **51**, 2300208 (2015).
- [20] V. Anishchenko, S. Nikolaev, and J. Kurths, *Phys. Rev. E* **73**, 056202 (2006).
- [21] M. Katsuragawa and T. Onose, *Opt. Lett.* **30**, 2421 (2005).
- [22] A. Zhang, X. Feng, M. Wan, Z. Li, and B. Guan, *Opt. Express* **21**, 12874 (2013).
- [23] C. W. Chow, C. S. Wong, and H. K. Tsang, *IEEE LEOS* **2**, 682 (2003).
- [24] L. Y. Chan, S. L. Fung, S. H. Wong, Y. K. Chan, F. Tong, L. K. Chen, and S. Y. Cheung, CLEO/Pacific Rim (2001), doi:10.1109/CLEOPR.2001.971083.
- [25] B. Nakarmi and Y. H. Won, SPIE Newsroom (2011), doi:10.1117/2.1201112.003914.
- [26] C. Su, L. Wang, S. Liaw, and Y. Huang, *Opt. Fiber Technol.* **16**, 1 (2010).
- [27] M. Geiser, C. Pflugl, A. Belyanin, Q. Wang, N. Yu, T. Edamura, M. Yamanishi, H. Kan, M. Fischer, A. Wittmann, J. Faist, and F. Capasso, *Opt. Express* **18**, 9900 (2010).
- [28] A. Hamadou, S. Lamari, and J.-L. Thobel, *J. Appl. Phys.* **114**, 203102 (2013).
- [29] C. Wang, F. Grillot, V. Kovanis, and J. Even, *J. Appl. Phys.* **113**, 063104 (2013).
- [30] M. M. Sheikhey, R. Yadipour, and H. Baghban, *Ann. Phys.* **530**, 1800079 (2018).